Local SAR Estimation via Electrical Properties Tomography: Physical Phantom Validations at 7T

Xiaotong Zhang[1], Jiaen Liu[1], Pierre-Francois Van de Moortele[2], and Bin He[1,3]

[1]*Department of Biomedical Engineering, University of Minnesota, Minneapolis, Minnesota, United States,* [2]*Center for Magnetic Resonance Research, University of Minnesota, Minneapolis, Minnesota, United States,* [3]*Institute for Engineering in Medicine, University of Minnesota, Minneapolis, Minnesota, United States*

AUDIENCE: RF pulse designers, RF Coil engineers, Electromagnetic Model builders, MR Physicists, Radiologists.

PURPOSE: International safety guidelines impose maximum global and local (averaged over 10 grams of tissue) limits on specific absorption rate (SAR), which is usually derived from lengthy numerical simulations using generic human body models. Electrical properties tomography (EPT)[1-4] is a recently introduced approach holding strong promises towards subject-specific local SAR computation based on B1 measurements. The purpose of the present work is to validate such B1-based local SAR estimation by using previously proposed gEPT algorithm[5]. B1 measurement was obtained in phantoms containing gelatin or biological tissues at 7T with a 16-channel transmit/receive coil, and local SAR distribution was predicted for a specific heating protocol. SAR results were subsequently converted into temperature changes which in turn were validated against temperature measurement based on MRI Thermometry.

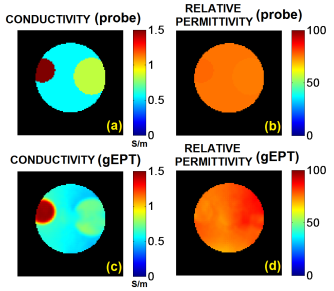

Fig.1. Gelatin phantom: (a)(b) probe-measured EP, (c)(d) reconstructed EP.

METHODS: A cylindrical gelatin phantom (12cm in radius and 20cm in height) with two balloons inserted was constructed; the container and two balloons were filled with a mixture of H_2O, $Cu_2SO_4 \cdot 5H_2O$ and different concentrations of NaCl. Another phantom was built using the same cylindrical container with one piece of porcine muscle and chicken breast inserted and saline gelatin solution filled. Bench measurements of EP were conducted with an Agilent 85070E dielectric probe kit and an Agilent E5061B network analyzer at 298MHz, and the heat capacity was measured with a KD2 Pro probe (Pullman, WA, USA) for each compartment of solution/tissue. Both phantoms were imaged in a 7T scanner (Magnetom 7T, Siemens, Erlangen, Germany) equipped with an elliptical 16-channel head transceiver coil[6]. Twelve contiguous transverse slices were sampled at a spatial resolution of 1.5×1.5×3mm^3.

MRI thermometry based on the proton chemical shift (PRF)[7] has been performed. Three cylinders of mineral oil were attached to the surface of the phantoms for phase drift corrections[8]. B1 phase shim setting (B1-shim I) was employed with stronger B1 in the periphery (CP2+ like mode). RF heating was achieved using an MR sequence consisting of 2ms square-shaped pulses applied every 200ms for a total duration of 3min without any encoding gradient. According to a PRF shift coefficient of -0.01 ppm/°C (for water-based solution and aqueous tissue[8]), the local temperature changes (ΔT_{PRF}) were derived from the measured phase maps acquired using a 3D GRE sequence (TE=10ms, TR=15ms, GRAPPA[9] acceleration x2, acquisition time 30s). For local SAR estimation, hybrid B1 mapping technique was applied as described in literature[10-12] under B1-shim I, the electrical properties distribution on each slice was reconstructed by employing gEPT[5], and the voxel-wise local SAR for the shimmed excitation was estimated as described previously[3], and averaged into a regional SAR value in 10 grams of tissue. Given the limited period of time t (up to several minutes) after starting RF-heating, thermal conduction was negligible, and the temperature increase ΔT within the static gelatin solution over time t can be treated as proportional to the induced local SAR as $\Delta T = t \cdot SAR / C_{phantom}$[8]. Therefore, B1-based temperature change (ΔT_{gEPT}) can be calculated directly from estimated local SAR values. Additionally, for the gelatin phantom, another B1 phase shim setting (B1-shim II) was employed, with the corresponding RF heating and MRI thermometry protocols repeated. For the SAR based temperature change estimation, however, B1 maps were only obtained using B1-shim I, and the resultant B1 map using shim II can be deduced knowing the altered B1 phase of individual channels. Based on this acquisition, ΔT_{gEPT} was first predicted for B1-shim setting I, and then ΔT_{gEPT} for B1-shim setting II was predicted based on the same measurement but taking the phase alteration from B1-shim I to II into account during the SAR calculation step.

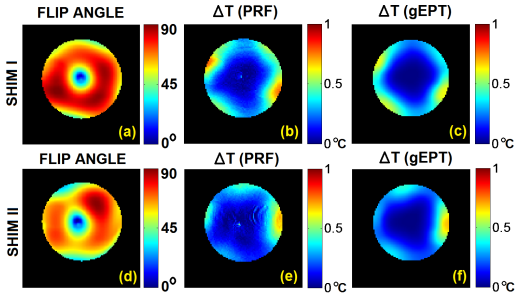

Fig.2. Gelatin phantom: under B1-shim I, (a) measured flip angle, (b) measured temperature change by PRF, and (c) predicted temperature change estimated from B1 measurement; under B1-shim II, (d) measure flip angle, (e) measured temperature change by PRF, (f) predicted temperature change estimated from B1 measurement under B1-shim I.

RESULTS: *Gelatin phantom* – On the transverse slice of interest (slice #6), reconstructed EP distributions using gEPT are shown in Fig.1 as compared to probe measurement. Under B1-shim I, Fig.2(a) shows measured flip angle, (b) measured temperature change $\Delta T_{PRF,shimI}$, and (c) predicted $\Delta T_{gEPT,shimI}$. A similarity can be observed between the latter two, including two regional hot spots in the periphery. Taking $\Delta T_{PRF,shimI}$ as the reference, for regions with measured $\Delta T_{PRF,shimI}$ larger than 0.1°C (arbitrarily chosen for a higher sensitivity in MRI thermometry), $\Delta T_{B1,shimI}$ exhibits a correlated distribution with a correlation coefficient (CC) of 0.8798 and mean relative error (RE) of -8.05%. Within the two regional hot spots located at 4 and 10 o'clock, the maximum values in $\Delta T_{PRF,shimI}$ measurement were 0.78°C and 0.78°C, versus the corresponding values in $\Delta T_{gEPT,shimI}$ prediction of 0.62°C and 0.61°C, respectively. Under B1-shim II, comparing measured $\Delta T_{PRF,shimII}$ in Fig.2(e) with predicted $\Delta T_{gEPT,shimII}$ in Fig.2(f) calculated from B1 measurement under B1-shim I, the corresponding CC is 0.8968 and RE of -0.42%, and the maximum value at the hot spot located at 3 o'clock is 0.71°C in $\Delta T_{PRF,shimII}$, versus 0.69°C in $\Delta T_{gEPT,shimII}$, respectively. *Tissue phantom* – Measured and estimated results are summarized in Fig.3. using aforementioned metrics, comparing measured ΔT_{PRF} in Fig.3(f) with predicted ΔT_{gEPT} in Fig.3(g), the corresponding CC is 0.8719 and RE of -23.18%, and the maximum value at the hot spot located at 1 and 7 o'clock is 0.66°C and 0.96°C in ΔT_{PRFI}, versus 0.37°C and 0.96°C in ΔT_{gEPT}, respectively.

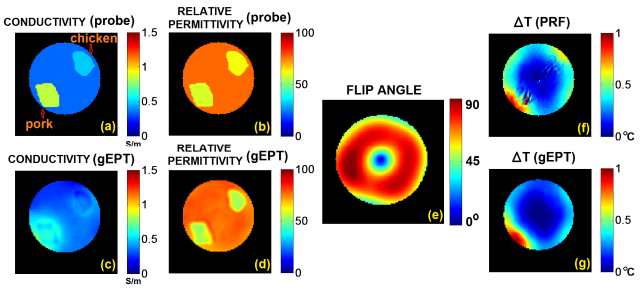

Fig.3. Tissue phantom: (a)-(b) probe-measured EP, (c)-(d) reconstructed EP, (e) measured flip angle, (f) measured temperature change by PRF, (f) predicted temperature change estimated from B1 measurement.

Discussion: In general, predicted ΔT_{gEPT} through gEPT preserves similar spatial pattern with high and low SAR regions as compared to those in ΔT_{PRF}; however, overall lower values are observed at hot spots in ΔT_{gEPT} maps especially in gelatin phantom experiment, which, as discussed in [13], may be due to the employed PRF shift coefficient[14] and the assumption of a dominant z-component of electric fields compared to their transverse components. **Conclusion:** It has been demonstrated that gEPT holds promises for enabling the use of subject-specific local SAR computation which in turn can be used as explicit constraint in shimming calculation as well as in parallel transmission RF pulse design.

References: 1) Katscher, IEEE TMI 28:1365. 2) Zhang, MRM 69:1285. 3) Zhang, IEEE TMI 32:1058. 4) Sodickson, ISMRM'12 387. 5) Liu, MRM'14 online. 6) Adriany, MRM 59:590. 7) Ishihara, MRM 34:814. 8) Oh, MRM 63:2186. 9) Griswold, MRM 47:1202. 10) Yarnykh, MRM 57:192. 11) Van de Moortele, MRM 54:1503. 12) Van de Moortele, ISMRM'07 1676. 13) Zhang, APL'14 in press. 14) Boulant, ISMRM'14 4900.

Acknowledgment: NIH R21EB017069, R01EB006433, R21EB009133, R21EB014353, P30NS057091, U01HL117664, P41EB015894 and S10 RR026783 of WM KECK Foundation. We thank Drs. Xiaoping Wu, Sebastian Schmitter, Nicolas Boulant, and Mr. Yicun Wang for useful discussion.